

OPTICAL METHOD BASED ON A GASEOUS SCINTILLATOR FOR NEUTRON ENERGY SPECTRUM MEASUREMENTS

Guanying Wang ^{1*}, Lijun Zhang ¹, Wengang Song ¹, Lingxin Chen ¹, Qiang Li ^{1,4}, Zhanqi Zheng ¹, Ran Han ², Xiaoping Ouyan ³

¹ Institute of Microelectronics, Chinese Academy of Sciences, Beijing, 100029, China; e-mail: wangguanying@ime.ac.cn

² Beijing Institute of Spacecraft Environment Engineering, Beijing, 100029, China

³ Northwest Institute of Nuclear Technology, Xi'an, 710024, China

⁴ Anhui University, Hefei, 230601, China

The neutron energy spectrum is one of the most important characteristic parameters. A novel optical measurement method is proposed. The purpose of the method is to determine the neutron spectra according to the recoil proton track length. The recoil protons deposit energy along the track and excite scintillator luminescence. The luminescence image directly reflects the neutron energy spectra. The Geant4 simulation toolkit is used to study the characteristics of the recoil proton luminescence distribution and determine the detector system response. A reconstruction algorithm based on the potential reduction interior point is developed and applied to spectrum unfolding. This method has the advantages of an intuitive measurement, good energy resolution, suitability for various charged particle beams, a wide energy range, convenience, and an adjustable range.

Keywords: optical method, neutron energy spectrum, gaseous scintillator, unfolding.

ОПТИЧЕСКИЙ МЕТОД ИЗМЕРЕНИЯ ЭНЕРГЕТИЧЕСКОГО СПЕКТРА НЕЙТРОНОВ НА ОСНОВЕ ГАЗОВОГО СЦИНТИЛЛЯТОРА

G. Wang ^{1*}, L. Zhang ¹, W. Song ¹, L. Chen ¹, Q. Li ^{1,4}, Zh. Zheng ¹, R. Han ², X. Ouyang ³

УДК 535.37;539.125.5

¹ Институт микроэлектроники Китайской академии наук, Пекин, 100029, Китай; e-mail: wangguanying@ime.ac.cn

² Пекинский институт инженерной экологии космических аппаратов, Пекин, 100029, Китай

³ Северо-Западный институт ядерных технологий, Сиань, 710024, Китай

⁴ Университет Анхой, Хэфэй, 230601, Китай

(Поступила 29 августа 2019)

Предлагается метод оптических измерений для определения нейтронных спектров по длине трека протона отдачи. Протоны отдачи выделяют энергию вдоль трека и возбуждают люминесценцию сцинтиллятора. Изображение люминесценции напрямую отражает энергетические спектры нейтронов. Набор инструментов моделирования Geant4 используется для изучения характеристик распределения люминесценции протонов отдачи и определения отклика детекторной системы. Разработан алгоритм восстановления, основанный на внутренней точке потенциальной редукции, который применяется для развертки спектра. Метод обладает преимуществами интуитивного измерения, хорошего разрешения по энергии, пригодности для различных пучков заряженных частиц, широкого диапазона энергий, удобства и регулируемого диапазона.

Ключевые слова: оптический метод, энергетический спектр нейтронов, газовый сцинтиллятор, разворачивание.

Introduction. The neutron energy spectrum carries a large amount of information about the characteristics of the nuclear reaction system and occupies a highly important position in the diagnosis of the radiation field [1]; it is the most direct and important means for the diagnosis of a pulsed radiation field. For example, neutron spectra in fusion plasmas can provide diagnostic information about the production mechanisms of the emitted neutrons and the energy distributions (keV) of the reacting ions [2] ($\Delta E_{D-D} = 82.5(T_{\text{ion}})^{1/2}$, $\Delta E_{D-T} = 177(T_{\text{ion}})^{1/2}$). Thus, it is possible to directly judge whether there is nonequilibrium combustion in the fusion process.

At present there are many ways to diagnose a pulsed neutron spectrum [3–7]. However, the high-energy-resolution measurement in some special radiation fields remains a problem [8, 9]. For the long pulse duration generated by a low-intensity and wide-pulse neutron source or a high-intensity steady neutron source, especially in situations where there is a small operating space or real-time measurement requirements [10], no suitable method has been developed. The time-of-flight method is no longer applicable owing to the long duration of the pulse [3, 4]. The counting spectrometer will fail because of the simultaneous arrival of large numbers of particles [8, 11]. The magnetic analysis method has a high energy resolution but a low detection efficiency and a complex structure [5, 6].

The purpose of this paper is to establish a set of energy spectrum measurement technologies based on an optical method. The track detector has intuitive features and can be applied to a pulsed radiation field [12, 13]. These features are combined with the advantages of real-time image information acquisition and the processing of a modern imaging module [14, 15]. For the new optical method, we introduce the basic concept and principle of recoil proton luminescence imaging and investigate its features. Then, the neutron energy test spectra from unfolding images are reported, and the unfolding solution results show the good performance of this optical method. In summary, this optical method is intuitive, accurate, and robust for neutron energy spectrum measurements.

Principle and simulation. Neutron detection has always maintained a special status in nuclear radiation detection technology. Neutrons have no charge, are difficult to detect, and are generally detected via nuclear reactions that convert neutrons into energetically charged particles. The optical detection method uses the recoil proton measurement principle and converts neutrons into recoil protons by a polyethylene target. The entire process is depicted in Fig. 1. For neutrons incident on a polyethylene target after collimation, the recoil proton beam is incident on the gaseous scintillator, and the protons are deposited along the track and excite scintillator luminescence. Then, we can obtain the neutron spectrum according to the scintillation image unfolding.

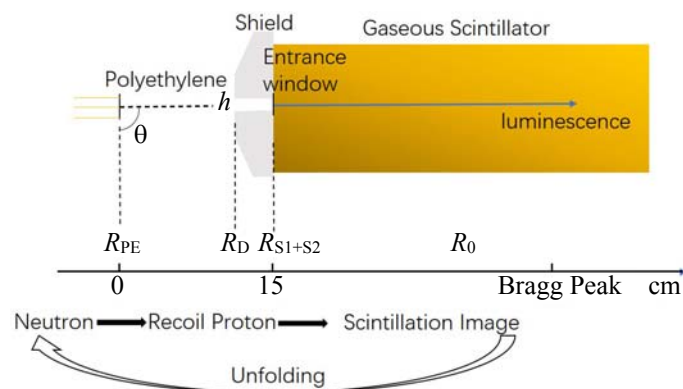


Fig. 1. Schematic diagram.

Gaseous scintillator. Gaseous scintillators are generally noble gases. The decay time is very short, usually several nanoseconds. Its properties are stable and can be easy to purify. By adjusting the pressure and changing the stopping power, gaseous scintillators can be applied to many kinds of charged particles with different energies and types. The gas density is approximately 3 to 4 orders of magnitude lower than that of solid (liquid) materials. Therefore, the track length of charged particles with the same energy difference can be clearly distinguished in gases, which can be achieved with a very fine energy resolution. Most importantly, a noble gas as a scintillator exhibits a fairly linear relationship between the luminous intensity and the particle energy [16]. The luminescence intensity of gaseous scintillators is proportional to the energy deposition for a wide range of particle energies E and stopping powers dE/dx .

We use a gas mixture of 90% Ar and 10% CF₄, with a pressure of 4.053 bar. The emission spectra of the primary scintillation from pure Ar are mainly in the ultraviolet region. It is improved by adding 10% CF₄, which allows the emission spectra to be distributed in both the ultraviolet region and the visible to near-infrared region [17]. This is suitable for the following optical device readout. The purpose of pressurization is to shorten the incident particle range. If the gas pressure is too low, a longer range is needed to fully deposit the energy. In fact, the kind of doped gas, concentration, and pressure can also be adjusted according to the actual situation. As long as the luminescence characteristics of the incident particles are particularly obvious, the energy of the recoil proton can be characterized.

The geometry and physical process of the detection system are constructed in the Geant4 toolkit. Geant4 is a package developed by CERN to simulate the performance of detectors in nuclear and high-energy physics [18]. The basic structure is described in the previous section. The simulation parameters are follows: for detector $R_{RE} = 0.2$ mm, $R_D = 100$ mm, $R_{S1+S2} = 50$ mm, $R_G = 700$ mm, $\theta = 0^\circ, -15^\circ, h = 10$ mm; for source particle neutron, type monoenergetic, energy 6 MeV, position (0, 0, -10 mm), direction (0, 0, 1). A typical luminescence distribution is shown in Fig. 2. The intensity of the luminescence presents an obvious Bragg curve distribution with respect to the incident recoil proton energy. There is a one-to-one match between the neutron energy spectra and luminescence distribution. The response matrix can be constructed by obtaining the luminescence distribution from a series of monoenergetic neutrons.

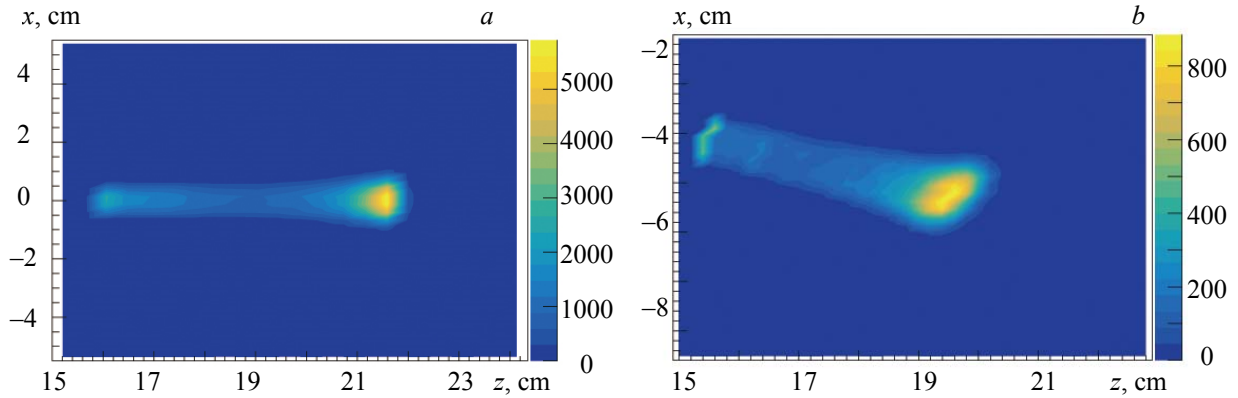


Fig. 2. Scintillation luminescence distribution of recoil protons generated by 6 MeV neutrons, the gaseous scintillator placed at 0° (a) and -15° (b).

Energy response linearity and energy resolution. The energy response linearity refers to whether there is a good linear relationship between the scintillator luminescence response and the neutron energy. By determining the variation in the luminescence intensity along the recoil proton incident direction, the position of the maximum luminescence intensity is employed to indicate the luminescence response. It is the position of the Bragg peak and is approximately the range of the recoil proton. In Geant4, a series of incident monoenergetic neutrons is employed to obtain the scintillation luminescence images (neutron energy: 4–16 MeV). Curves of the linearity of the energy response are fitted in Fig. 3a. Similarly, the luminescence intensity versus deposited energy is also obtained in Fig. 3b. Because of the excellent luminescence properties of gases, the energy response shows good linearity. In practice, neutron energy spectra are determined according to both the range length and scintillation luminescence distribution. The track of the range length calibrates the energy, while the luminescence intensity calibrates the intensity of the corresponding energy.

The energy of the incident particles is distinguished based on the scintillation luminescence image distribution. The purpose of this approach is to determine the energy difference ΔE according to the range difference ΔR of the particle beam:

$$\Delta E = \int_0^{\Delta R} - (dE / dx) dx. \quad (1)$$

Therefore, the energy resolution is determined by the minimum track difference of the particle beam in the gas. It is worth mentioning that the energy resolution is also seriously affected by the polyethylene target, entrance window, and spectrum unfolding algorithm. These factors all can cause energy straggling. The exact energy resolution is closely related to the measurement conditions. Here, we are only discussing the energy resolution caused by scintillation gas. Modern CCD/CMOS cameras are an effective imaging means

that have a good position resolution within tens of micrometers in each pixel [12, 19, 20]. We assume that at least one pixel is needed to distinguish two images. This value of $160\ \mu\text{m}$ is the limit for converting the position resolution to the corresponding energy resolution. As shown in Fig. 4, the optical method can distinguish the energy difference within 20 keV. We add the result of 3 MeV for complete analysis. It can be concluded that the energy resolution improves with increasing energy. This is because of the larger energy, the larger difference in range, and ease of distinguishing. The energy resolution of this optical method is strongly dependent on energy, which is suitable for high energy neutron measurement. The typical values are $9.05\ \text{keV} - 4\ \text{MeV}$, $3.28\ \text{keV} - 10\ \text{MeV}$, and $2.2099\ \text{keV} - 16\ \text{MeV}$.

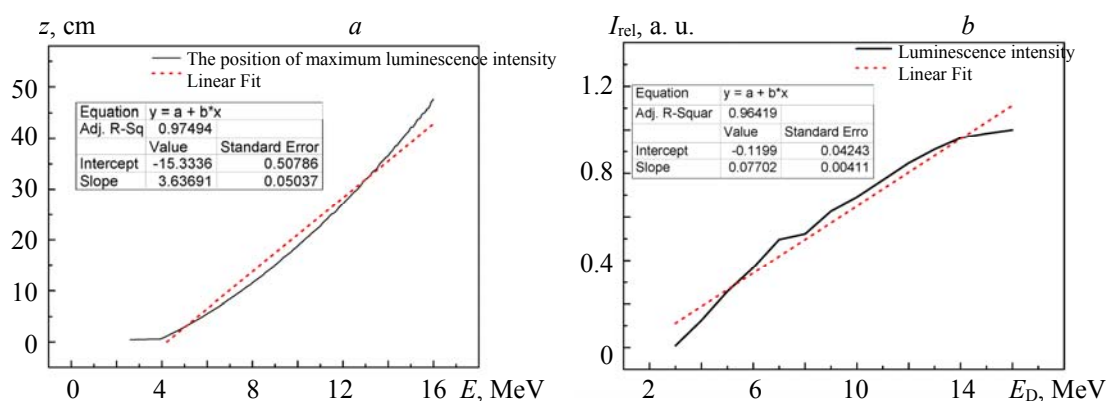


Fig. 3. Linearity of the energy response (a) and luminescence intensity versus the deposited energy (b).

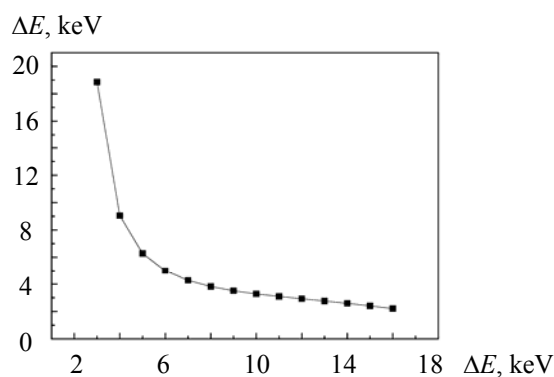


Fig. 4. Minimum distinguishable energy difference in scintillation gas.

In addition, the energy loss and scattering caused by the polyethylene target are approximately 90 keV [21], the energy broadening of the entrance window, air, and other structures is approximately 40 keV [22], and the spectrum unfolding algorithm accuracy is approximately 0.4–1.0% [23]. Thus, the energy resolution of the whole detection system is estimated to be no more than 5%.

Detection efficiency. The detection efficiency of this optical method is affected by the following factors: first, the recoil proton yield, which depends on the thickness of polyethylene target and neutron energy; second, the receiving angle, which is determined by the relative position of the detector; third, the scintillator light output and its acquisition, which is related to the physical structure of the detection system and the performance of the optical device readout. Specifically, the geometric size and structural materials of the detection system, the composition, and the pressure of the scintillation gas determine the scintillation performance. For the optical device readout, the sensitive band should be able to cover the scintillation light wavelength range.

The detection efficiency is defined by the ratio of the total number of detected scintillations generated by the recoil protons into the gas to the total number of incident collimated neutrons. Figure 5 shows the results where, as the neutron energy increases, the detection efficiency decreases slightly. Overall, the detection efficiency is about 10^{-4} . The detection efficiency of this optical method has little dependence on energy, and the typical values are $2.1784 \times 10^{-4} - 4\ \text{MeV}$, $1.3878 \times 10^{-4} - 10\ \text{MeV}$, and $1.0096 \times 10^{-4} - 16\ \text{MeV}$.

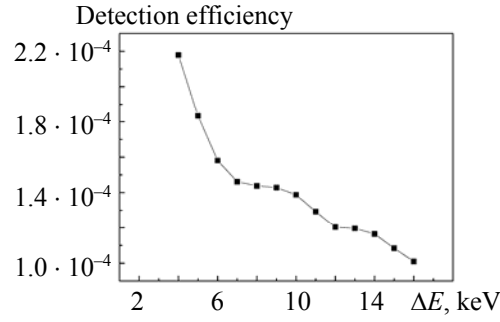


Fig. 5. Detection efficiency.

The detection efficiency can be improved by appropriately increasing the thickness of polyethylene target, enlarging the receiving angle, using multi-directional measurement, or adjusting the scintillation performance by changing the gas composition. Therefore, it is suitable for many situations, from low yield to high yield measurements.

Methods and test. Response matrix. The basic principle of unfolding is to determine the real neutron energy spectra from the luminescence distribution. This equation can be written as a Fredholm integral function of the first kind:

$$\varphi(z) = \int_{E_{\min}}^{E_{\max}} R(E, z) N(E) dE, \quad (2)$$

where z denotes the track length and E denotes the neutron energy; $\varphi(z)$ denotes the scintillation luminescence intensity along the recoil proton incident direction; $N(E)$ denotes the neutron energy spectra, and $R(E, z)$ is the detector response function. The response includes three main stages as follows:

$$R(E, z) = R_{n-p}(E, E_p) R_{\text{loss}}(E_p, E_p') R_{\text{scint}}(E_p', z), \quad (3)$$

where E_p is the recoil proton energy and E_p' is the recoil proton energy after scattering and energy loss; R_{n-p} , R_{loss} , and R_{scint} are the proton conversion, energy loss, and scintillation luminescence, respectively.

Unlike the recoil proton track imaging mentioned in [24], the neutron energy is obtained by two steps in which the recoil proton energy is obtained from the scintillation luminescence image unfolding, then converted to the neutron energy. In this paper, the neutron energy spectrum is directly unfolded from the scintillation luminescence image. The response matrix R includes all intermediate processes. It is no longer necessary to calculate each step separately.

If we break E and z into discrete intervals, the integral Eq. (2) is rewritten as a discrete matrix as:

$$\varphi_i = \sum R_{ij} N_j, \quad (4)$$

where N_j represents the neutron energy spectrum in discrete form, and j is the energy group number; φ_i is similar. When the energy group numbers i and j are large enough, Eq. (4) can be replaced by Eq. (2).

To unfold the measured neutron energy spectrum, it is required to know precisely the detector response $R(E, z)$. The response matrix can be obtained by a Monte Carlo simulation. The detector response is shown in Fig. 6.

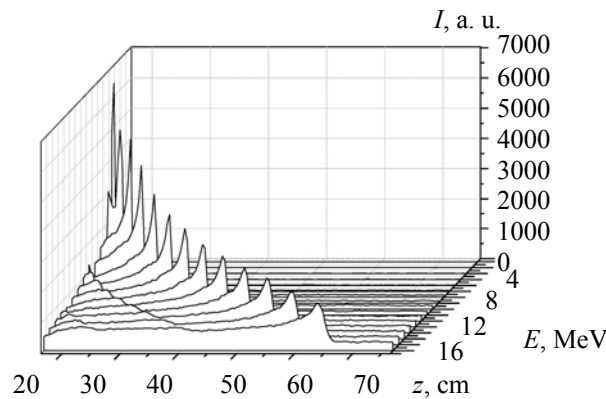


Fig. 6. Detector response curve for monoenergetic neutrons (neutron energy 4–16 MeV).

Unfolding algorithm. In general, unfolding the neutron energy spectrum is very difficult. The response of the detector R_{ij} is usually ill conditioned, so minute perturbations can cause large fluctuations in the solution. In addition, a Fredholm integral function of the first kind is a typical ill-posed problem, and a solution may not exist, or a solution may exist but is not unique or depends on the initial conditions.

A potential reduction interior point algorithm (PRIP) is developed based on the widely used interior-point algorithm. The basic concept is to adjust the iteration step such that it satisfies the solution of the linear complementarity problem; at the same time, the potential function value is decreased. This algorithm is stable and provides efficient, accurate results [25].

A brief introduction is given as follows. First, we transform the inverse problem in Eq. (4) into a least-squares problem:

$$\min_{x \in R} f(x) = Ax - b^2, \quad (5)$$

where $A \in R^{m \times n}$ ($m \geq n$), and $b \in R^m$, $x \in R^n$.

Then, the potential function is constructed:

$$\Phi(x, y) = (n + \rho) \log(x^T y) - \sum_{i=1}^n \log(x_i y_i) - n \log(n), \quad (6)$$

where ρ is the iterative parameter and n is the matrix order. Assume that $M = A^T A$, $q = -A^T b$, and $y = Mx + q$. Note that $S_{++} = \{(x, y) : y = Mx + q, x > 0, y > 0\}$ is the strictly feasible interior point to get the iteration step λ .

$$\begin{cases} (x + \lambda \Delta x, y + \lambda \Delta y) \in S_{++} \\ \Phi(x + \lambda \Delta x, y + \lambda \Delta y) - \Phi(x, y) \leq -\delta \end{cases}, \quad (7)$$

where δ is the parameter.

The iteration direction $(\Delta x, \Delta y)$ depends on the solution of the Newton direction and central path direction simultaneous equation group:

$$\begin{cases} y \Delta x + x \Delta y = h \\ -M \Delta x + \Delta y = 0 \end{cases}, \quad (8)$$

where $h = -[xy - \beta(x^T y/x)e]$ and $\beta = n/(n + \rho)$. The termination condition is $(x^k)^T y \leq \varepsilon$. Finally, the optimal solution is x^k .

According to the theoretical derivation, when the parameter of the potential function $\rho = O\sqrt{n}$, the solution of (x^k, y^k) can be obtained after at most $O(\sqrt{n} \log(\varepsilon^{-1} 2^{\Phi(x_0, y_0)/\rho}))$ times iteration.

Compared with the widely used GRAVEL algorithm, the PRIP algorithm is highly computationally efficient and fast converging. It is suitable for solving the unfolded problem of large computational complexity.

Results and discussion. To verify this optical method, several neutron energy spectra with multipeak and Gaussian distributions are used as a test. Their scintillation luminescence images are shown in Figs. 7a,c. Also shown in Figs. 7b,d is the luminescence intensity along the incident energy direction, which is extracted as input data for the unfolding.

Figure 8 shows the unfolding solution results. Figure 8a shows the results of a neutron energy spectrum with two peaks at 6 and 8 MeV, for which the intensity ratio is 1:1. Figure 8b shows the results of a Gaussian neutron energy spectrum with $\sigma = 0.18$ MeV and $\mu = 10.0$ MeV. The unfolding solution results are consistent with the real spectra.

We define Q_s and Q_r to evaluate the accuracy of the unfolded solution results as follows [26]: N_i and $N_{i,\text{real}}$ represent the solution results and the real energy spectrum, respectively; φ_i is derived from the solution results N_i according to Eq. (4) ($\varphi_i = RN_i$); φ_i is derived in a similar manner. Obviously, a perfect unfolded result would match the real spectrum exactly and give $Q_s = Q_r = 0$.

$$Q_s = \left[\frac{\sum_{i=1}^n (N_i - N_{i,\text{Real}})^2}{\sum_{i=1}^n (N_{i,\text{Real}})^2} \right]^{\frac{1}{2}}, \quad Q_r = \left[\frac{\sum_{i=1}^n (\varphi_i - \varphi_{i,\text{Real}})^2}{\sum_{i=1}^n (\varphi_{i,\text{Real}})^2} \right]^{\frac{1}{2}}. \quad (9)$$

The accuracy of the evaluation for the unfolded solution results is follows: Multi-peak (Fig. 8a) $Q_s = 0.050200$, $Q_r = 14.522419$; Gaussian (Fig. 8b) $Q_s = 0.225167$, $Q_r = 7.357397$. The values of Q_s and Q_r are very small. Although the Q_s value of the multipeak spectrum is better, the Q_r value of the Gaussian spec-

trum is better. Overall, the results closely match the real spectra. It is found that the optical method is stable and provides efficient, accurate results.

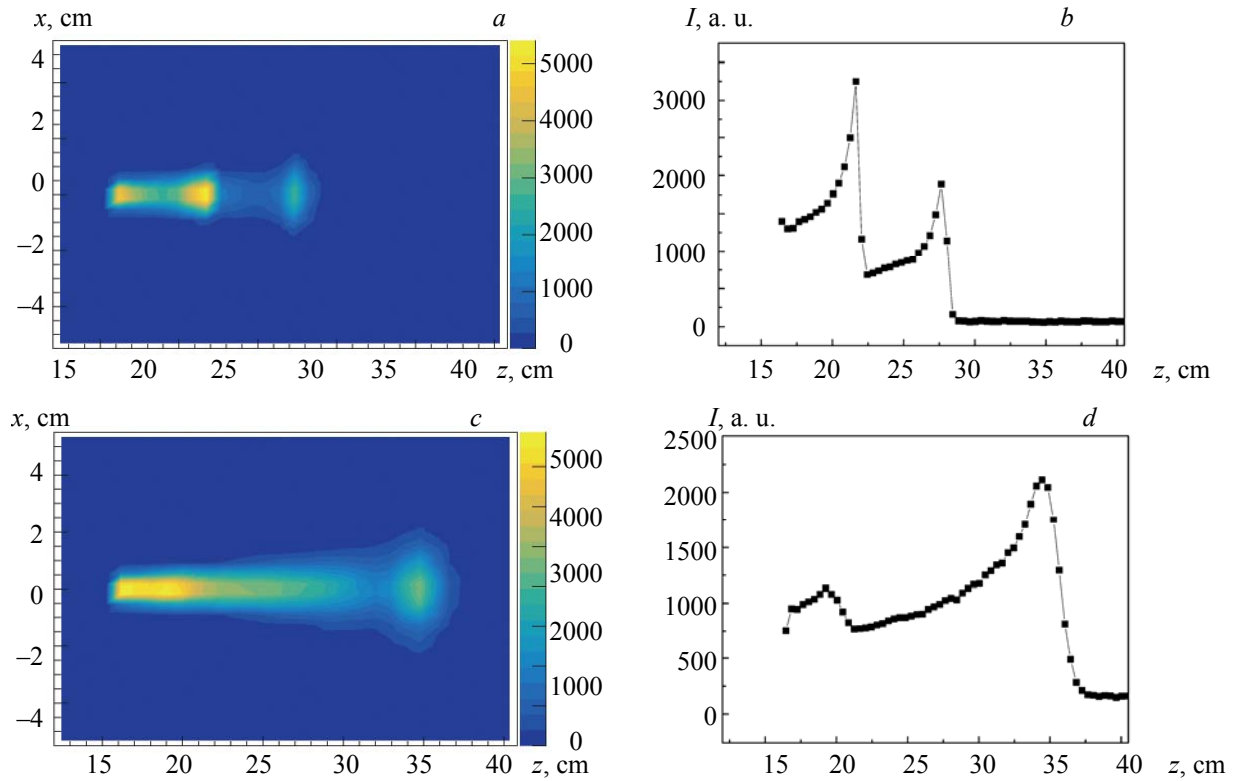


Fig. 7. Scintillation luminescence distribution with a multippeak neutron energy spectrum (a, b) and a Gaussian neutron energy spectrum (c, d). a) The overall scintillation luminescence image; b) the luminescence intensity along the incident direction; c) the neutron energy spectrum with two peaks at 6 and 8 MeV, for which the intensity ratio is 1:1; d) the Gaussian neutron energy spectrum with $\sigma=0.18$ MeV and $\mu=10.0$ MeV.

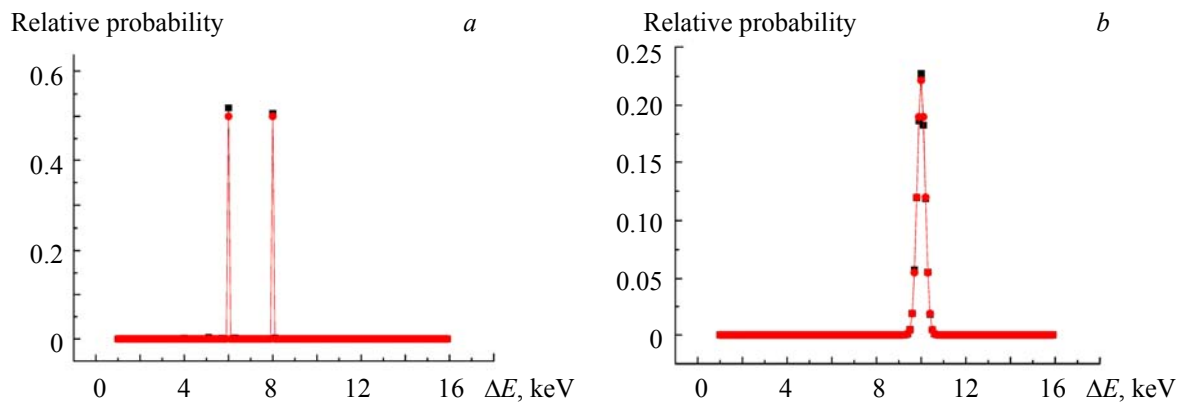


Fig. 8. The real (\bullet) and the unfolded (\blacksquare) neutron energy spectrum with two peaks at 6 and 8 MeV, for which intensity ratio is 1:1 (a), and the Gaussian neutron energy spectrum with $\sigma=0.18$ MeV, $\mu=10.0$ MeV (b).

Conclusions. An optical readout method based on the recoil proton track length in a gaseous scintillator was proposed for a direct, real-time, and high-energy-resolution measurement of neutron fields. The proposed approach solves the shortcomings of existing methods, such as the complex structure and the

limitation of the intensity of the radiation field. This approach explores a new technical method for accurate energy spectrum measurements.

The basic idea was to use a polyethylene target as a converter and measure the scintillation luminescence distribution of recoil protons in a gaseous scintillator. The system was tested with monoenergetic neutrons, demonstrating linearity, a detection efficiency of about 10^{-4} , and energy resolution of no more than 5%. By using Monte Carlo simulations to build the response matrix, the measurements performed with multipeak and Gaussian distributions showed good agreement with the real neutron energy spectra. These validated the satisfactory performance of this optical method.

This work is a preliminary step in the study of optical methods. Future work will focus on how to use a 2-D distribution of the scintillation luminescence as input data for unfolding. A 2-D distribution of scintillation luminescence can provide more information about the neutron spectrum. A detailed analysis will be described in a separate paper.

Acknowledgments. Financial support from the Opening Foundation of State Key Laboratory of Intense Pulsed Radiation Simulation and Effect are gratefully acknowledged.

REFERENCES

1. N. O. Jarvis, *Plasma Phys. Controlled Fusion*, **36**, N 2, 209–244 (1994).
2. B. Wolle, *Phys. Rep.*, **312**, 1–86 (1999).
3. V. Y. Glebov, C. Stoeckl, T. C. Sangster, et al. *Rev. Sci. Instrum.*, **75**, N 10, 3559–3562 (2004).
4. Z. A. Ali, V. Y. Glebov, M. Cruz, et al. *Rev. Sci. Instrum.*, **79**, N 10, 3559 (2008).
5. D. T. Casey, J. A. Frenje, M. Gatu Johnson, et al. *Rev. Sci. Instrum.*, **84**, N 4, 043506 (2013).
6. D. T. Casey, J. A. Frenje, M. G. Johnson, et al. *Rev. Sci. Instrum.*, **83**, N 10, 10D912 (2012).
7. E. Mendoza, D. Cano-Ott, C. Guerrero, et al. *Nucl. Instrum. Methods Phys. Res. A*, **768**, 55–61 (2014).
8. Lénárd Pál, Imre Pázsit, *Nucl. Instrum. Methods Phys. Res. A*, **693**, 26–50 (2012).
9. M. J. Koskelo, W. A. Sielaff, D. L. Hall, et al. *J. Radioanal. Nucl. Chem.*, **248**, N 2, 257–262 (2001).
10. L. Chen, X. P. Ouyang, Z. B. Zhang, et al. *World Academy of Science, Engineering and Technology* (2011).
11. E. D. Bourret-Courchesne, S. E. Derenzo, M. J. Weber, *Nucl. Instrum. Methods Phys. Res. A*, **601**, N 3, 358–363 (2009).
12. G. Laczko, V. Dangendorf, M. Krämer, et al. *Nucl. Instrum. Methods Phys. Res. A*, **535**, N 1-2, 216–220 (2004).
13. U. Titt, A. Breskin, R. Chechik, et al. *Nucl. Instrum. Methods Phys. Res. A*, **416**, N 1, 85–99 (1998).
14. F. A. F. Fraga, L. M. S. Margato, S. T. G. Fetal, et al. *Nucl. Instrum. Methods Phys. Res. A*, **478**, N 1-2, 357–361 (2002).
15. F. A. F. Fraga, L. M. S. Margato, S. T. G. Fetal, et al. *Nucl. Instrum. Methods Phys. Res. A*, **513**, N 1, 379–387 (2003).
16. E. Aprile, A. E. Bolotnikov, A. I. Bolozdynya, T. Doke, *Noble Gas Detectors* (2006).
17. J. Liu, X. Ouyang, L. Chen, et al. *Nucl. Instrum. Methods Phys. Res. A*, **694** (Complete), 157–161 (2012).
18. J. Allison, et al. *Nucl. Instrum. Methods Phys. Res. A*, **835**, 186–225 (2016).
19. N. S. Phan, R. J. Lauer, E. R. Lee, et al. *Astroparticle Phys.*, **84**, 82–96 (2016).
20. I. Mor, D. Vartsky, V Dangendorf, et al. *J. Instrum.*, **12**, N 12, C12022 (2017).
21. J. Zhang, X. Ouyang, X. Zhang, et al. *Nucl. Instrum. Methods Phys. Res. A*, **816**, 125–130 (2016).
22. S. Agosteo, A. Fazzi, M. Introini, M. Lorenzoli, A. Pola, *Radiat. Measur.*, **85**, 1–17 (2016).
23. H. Shahabinejad, M. Sohrabpour, *Radiat. Phys. Chem.*, **136**, 9–16 (2017).
24. H. Jing, L. Jinliang, Z. Zhongbing, et al. *Sci. Rep.*, **8**, N 1, 13363 (2018).
25. G. Wang, R. Han, X. Ouyang, et al. *Chin. Phys. C*, **41**, N 5, 181–185 (2017).
26. D. W. Freeman, D. R. Edwards, A. E. Bolon, *Nucl. Instrum. Methods Phys. Res. A*, **425**, N 3, 549–576 (1999).